

The role of inertia in extensional fall of a viscous drop

By **Y. M. STOKES** AND **E. O. TUCK**

Department of Applied Mathematics, University of Adelaide, Australia.

(Received 18 February 2002)

In flows of very viscous fluids, it is often justifiable to neglect inertia and solve the resulting creeping-flow or Stokes equations. For drops hanging beneath a fixed wall and extending under gravity from an initial rest state, an inevitable consequence of neglect of inertia and surface tension is that the drop formally becomes infinite in length at a finite crisis time, at which time the acceleration of the drop, which has been assumed small relative to gravity g , formally also becomes infinite. This is a physical impossibility, and the acceleration must in fact approach the free-fall value g . However, we verify here, by a full Navier-Stokes computation and also with a slender-drop approximation, that the crisis time is a good estimate of the time at which the bulk of the drop goes into free fall. We also show that the drop shape at the crisis time is a good approximation to the true final shape of the freely-falling drop, prior to smoothing by surface tension. Additionally, we verify that the drop has an initial acceleration of g , which quickly decreases as viscous forces in the drop become dominant during the early stages of fall.

1. Introduction

Extensional flow and break-off of viscous fluid drops has been much studied (see the literature review in Stokes, Tuck & Schwartz 2000). In particular, fall under gravity of a drop of very viscous fluid hanging under a solid boundary, such as honey dripping from a spoon held upside-down, was examined in Stokes et al. (2000). Because of the high viscosity of the fluid, inertia and surface tension were assumed to be small relative to viscous and gravitational forces, and were therefore neglected. The resulting Stokes-flow problem was solved using both a slender-drop approximation and finite-element methods. However, neglect of inertia in the latter stages of the fall of the drop, when its acceleration is no longer small and in fact must eventually approach the free-fall value g , results in a finite “crisis” time at which the length and acceleration of the drop formally become infinite, simultaneously with its cross-sectional area becoming zero at some point along its length (often close to the solid boundary).

Wilson (1988) suggested for a similar problem that this non-physical infinity could be removed by putting inertia back into the problem, and also identified the crisis time with the time at which the drop breaks. Kaye (1991) considered some problems of viscous extensional flow with inertia, but did not discuss the effect of inertia on the crisis time or acceleration. Cram (1984) also studied falling drops numerically using a one-dimensional approximation. More recent references on drops that are falling and/or in extensional flow include Henderson et al. (2000), Wilkes, Phillips & Basaran (1999) and Sarkar & Schowalter (2001).

Clearly, inertia can only be justifiably neglected when the acceleration of the fluid in the drop is small compared to the gravitational acceleration g , and inclusion of inertia

terms in the equations of motion should lead to a solution that agrees more closely with reality. It is of interest to demonstrate this explicitly and so determine the time at which inertia begins to play a significant role, in the latter stages of the fall of the drop.

Actually, inertia must also be important in the very earliest stages of its fall. Neglect of inertia yields Stokes-flow equations which imply that the initial acceleration of the drop is infinite and that the drop starts with an impulsively-developed initial velocity. In practice, it must undergo an acceleration from rest of magnitude g , which is large compared to the fluid accelerations that apply soon after motion begins, when viscous retarding forces in the drop are dominant. Again the physics requires inclusion of inertia in any analysis of the very early stages of the flow, if we wish to estimate the true magnitude of the accelerations.

In the context of inertial influence on this extensional flow, the shape of the evolving drop is also of considerable interest. The shape as a function of time is non-trivially and uniquely determined by the drop's initial shape, and only after a relatively long time in free fall will surface tension mandate smoothing of that shape. When inertia is neglected as in Stokes et al. (2000), we are able to compute a drop shape up to but not beyond the finite crisis time. However, since we anticipate break-off at close to this time, the drop shape at crisis should be a good approximation to the subsequent shape of the freely falling drop.

On the other hand, as soon as inertia is included in the analysis, the computations can proceed beyond the crisis time of the inertia-less theory, into a regime where the physics demands that the main drop is nearly in free fall as a rigid body, except for a very thin extending filament connecting it to the wall. Then we can determine just how well the shape of this almost-rigid body compares with the drop shape at crisis time predicted by the inertia-less theory. In contrast to the inertia-less theory, with inertia included and in the absence of surface tension, the thin connecting filament never breaks, but becomes ever thinner and thinner as time increases. Such filaments can indeed be very long in practice for very viscous fluids, as a drop of honey shows, but for less viscous fluids, surface tension effects (neglected here) eventually play a role and cause the filament to break (Eggers 1993; Papageorgiou 1995).

Once inertia is included in the analysis we need not be restricted to highly viscous fluids, but may measure the influence of inertia by a Reynolds number R which is inversely proportional to the square of the viscosity. For small R we expect the drop behaviour to be well-approximated by the inertia-less theory, with the quality of this approximation decreasing as R increases. Meanwhile, as the fluid viscosity decreases, surface tension will also play a more significant role in drop behaviour, but we do not consider quantitative effects of surface tension in the present paper, concentrating our attention on the effects of inertia.

2. Mathematical formulation

We consider a drop of incompressible Newtonian fluid with density ρ and kinematic viscosity $\nu = \mu/\rho$, hanging beneath a horizontal surface at $x = 0$. The complete mathematical formulation is similar to that in Stokes et al. (2000), but with the addition of inertia. Thus, g acts in the x direction and the Navier-Stokes and continuity equations are given in Cartesian coordinates by

$$\frac{\partial \mathbf{q}}{\partial t} + \mathbf{q} \cdot \nabla \mathbf{q} = g\mathbf{i} - \frac{1}{\rho} \nabla p + \nu \nabla^2 \mathbf{q}, \quad (2.1)$$

and

$$\nabla \cdot \mathbf{q} = 0, \quad (2.2)$$

where $\mathbf{q} = (u, v, w)$ is the velocity vector, p is the pressure and \mathbf{i} is the unit vector in the x direction. We consider a drop that lies in $0 < x < L(t)$, where $x = 0$ is the wall boundary and $x = L(t)$ is the (to-be-determined) lower free end. The drop is assumed to be initially at rest with a given initial shape, having length $L_0 = L(0)$ and maximum width w_0 .

Equations (2.1) and (2.2) would usually be solved subject to no-slip boundary conditions at the wall $x = 0$ and zero-stress free-surface and kinematic conditions on all other boundaries (see Stokes et al. 2000). However, for a slender drop approximation, we must allow slip along the wall.

As already indicated, our main attention in the present paper is directed toward two matters, namely computation of the acceleration $L''(t)$ of the bottom point of the drop, and determination of the shape of the final freely-falling drop. Very small Reynolds numbers will give the best comparison with results from the inertia-less theory, but larger Reynolds numbers, i.e. less viscous fluids, display more clearly the large-time characteristics of a falling viscous fluid drop.

We consider both two-dimensional thin sheets and axisymmetric slender drops. In the absence of significant surface tension effects, these behave similarly, drop width in two dimensions being equivalent to drop cross-section area for axisymmetric drops. For extremely slender axisymmetric filaments, the large lateral curvature implies surface tension effects which are absent in the equivalent two-dimensional case, but these effects do not have any major influence on the main-drop behaviour over the time frame of interest here. Rather they are of interest in the study of pinch-off and rupture of the filament to release the main drop into actual free fall. Significantly, our work (both here with inertia and previously Stokes et al. (2000) without inertia), although neglecting surface tension, does give an indication of when and where the high-curvature factors causing filament rupture become important, and hence when and where break-off of the drop is likely to occur, without specifying the surface-tension-dependent details of this subsequent event.

The full flow problem defined above may be readily solved without approximation using finite elements, and we first do this to identify interesting features of the flow. Most (but not all) of these features are also captured by a semi-analytic slender-drop analysis to follow, by use of which we seek to better understand what is happening. An intuitive large-time asymptotic analysis for slender drops then gives an explicit formula connecting initial and final shapes, which is confirmed by the detailed computations.

3. Finite-element computations

A finite-element algorithm was described and used in Stokes et al. (2000) for computing the extension under gravity of a viscous drop, neglecting inertia. We need only modify this algorithm for the problem formulated above including inertia.

First note that, because of the Lagrangian time-stepping method, the non-linear nature of the inertia terms in the Navier-Stokes equations presents no difficulties. We simply discretise the acceleration $D\mathbf{q}/Dt = \partial\mathbf{q}/\partial t + (\mathbf{q} \cdot \nabla)\mathbf{q}$ following a particle, using backward Euler differencing so that (2.1) becomes

$$\mathbf{q}^{n+1} - \Delta t \left(g\mathbf{i} - \frac{1}{\rho} \nabla p^{n+1} + \nu \nabla^2 \mathbf{q}^{n+1} \right) = \mathbf{q}^n, \quad (3.1)$$

where Δt is the time-step size and \mathbf{q}^n and p^n are the velocity and pressure distributions in the flow domain at the n th time step, with $\mathbf{q}^0 = \mathbf{0}$. The continuity equation (2.2) is just

$$\nabla \cdot \mathbf{q}^{n+1} = 0. \quad (3.2)$$

Now, (assuming for the moment 2D flow) let a fluid particle be labelled by its initial position vector $\mathbf{r}^0 = (\xi, \eta)$, and let its position at time $t \geq 0$ be given by $\mathbf{r}(\mathbf{r}^0, t) = (x(\mathbf{r}^0, t), y(\mathbf{r}^0, t))$, with $\mathbf{r}(\mathbf{r}^0, 0) = (x(\mathbf{r}^0, 0), y(\mathbf{r}^0, 0)) = (\xi, \eta)$. In particular, ξ is the initial distance of the particle below the wall. Then we compute the subsequent displacement of this particle by backward differencing, i.e.

$$\mathbf{q}^{n+1} = \frac{d\mathbf{r}^{n+1}}{dt} = \frac{\mathbf{r}^{n+1} - \mathbf{r}^n}{\Delta t}, \quad (3.3)$$

where $\mathbf{r}^n = \mathbf{r}(\mathbf{r}^0, n\Delta t)$ is the particle position at the n th time step.

Thus our computational algorithm can be summarised as follows:

(a) construct a mesh of interconnected nodes over the fluid region, each node representing a fluid particle;

(b) set $n = 0$;

(c) use the finite-element method to solve the discretised forms of the Navier-Stokes and continuity equations (3.1), (3.2) for the velocity \mathbf{q}^{n+1} and pressure p^{n+1} at each of the mesh nodes, subject to the initial condition $\mathbf{q} = \mathbf{0}$ and no-slip and zero-stress conditions on the wall and free surface boundaries respectively;

(d) solve (3.3) for the new position vector \mathbf{r}^{n+1} of each mesh node;

(e) move each node to its new position;

(f) increment n and repeat steps c-e to obtain the time-evolution of the drop.

At time step $n = 1, 2, \dots$, we can compute the vertical component a^n of the fluid acceleration of a mesh node, i.e. of a fluid particle, by simple backward differencing,

$$a^n = a(\mathbf{r}^0, n\Delta t) = \frac{u^n - u^{n-1}}{\Delta t}, \quad (3.4)$$

where $u^n = u(\mathbf{r}^0, n\Delta t)$ is the x -component of velocity of the particle at time step n . In particular, the vertical acceleration $L''(n\Delta t)$, $n = 1, 2, \dots$, at the centre-bottom of the drop, is given by (3.4) with $\mathbf{r}^0 = (L_0, 0)$. Close to $t = 0$ we use a very small time step, but progressively increase this at larger times.

This algorithm has been implemented in the finite-element package *Fastflo*, CSIRO (1999), for both two-dimensional and axisymmetric drops. The symmetry of the drop enables us to use only half of the fluid domain. An augmented-Lagrangian method was used to solve for velocity and pressure (CSIRO 1999, pp. 165–169). Eventually the computations must cease because of excessive stretching of mesh elements leading to numerical inaccuracy and ultimately failure.

Results are presented in non-dimensional form using the length scale L_0 , a time scale $T = \nu^*/(gL_0)$, and a velocity scale $U = gL_0^2/\nu^*$, where $\nu^* = 4\nu$ in two dimensions and $\nu^* = 3\nu$ in three dimensions. This allows definition of a Reynolds number

$$R = \frac{UL_0}{\nu^*} = \frac{gL_0^3}{\nu^{*2}}. \quad (3.5)$$

Results for an initially-rectangular two-dimensional drop of aspect ratio $w_0/L_0 = 0.2$, for a very small Reynolds number $R = 0.001$ and a somewhat larger value $R = 0.1$, are shown in Figures 1 to 4. A mesh of 690 quadratic triangular elements was used, with elements clustered near the wall where there is most distortion from the initial shape. Computations were continued at least until the drop acceleration had (very nearly)

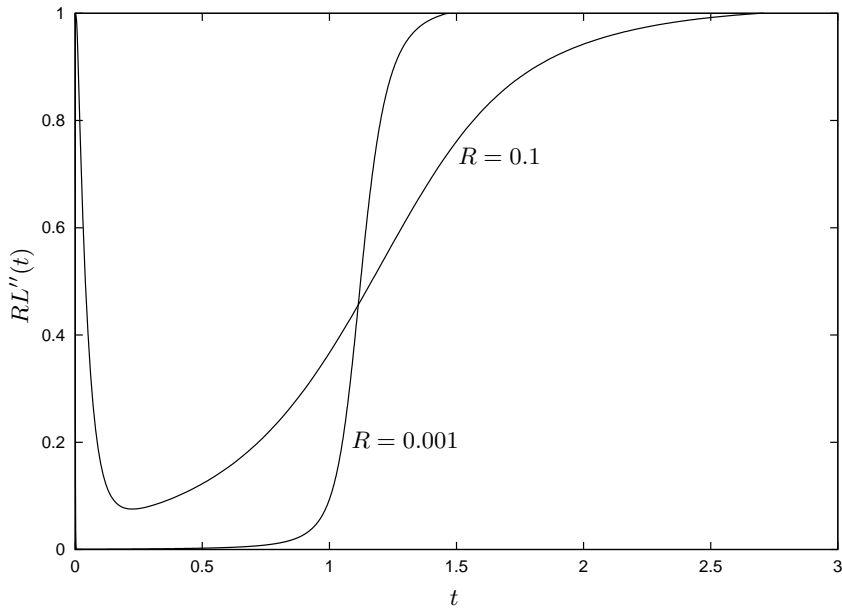


FIGURE 1. Vertical acceleration RL'' versus time t . Initially rectangular drop of aspect ratio $w_0/L_0 = 0.2$.

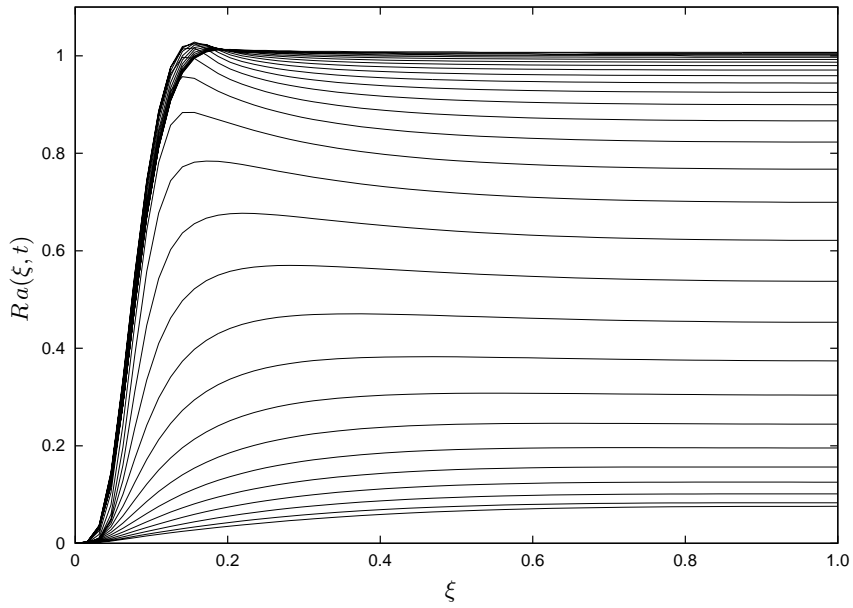


FIGURE 2. Acceleration as a function of initial position ξ along the drop centre line, $R = 0.1$, $t = 0.2, 0.3, \dots, 3.0$.

returned to g , but could not be taken too far beyond this time due to excessive mesh distortion.

3.1. Accelerations

The scaled vertical acceleration $RL''(t)$ of the bottom-most point of the drop, which is unity when the actual acceleration takes the value g , is plotted in Figure 1. As expected, the actual acceleration starts at g , falls rapidly to a small value while viscosity dominates, and then rises, returning to g at large times when the drop is effectively in free fall. The smaller the Reynolds number, the faster and larger is the initial drop in acceleration from g , the minimum value of $RL''(t)$ being of the order of R as is most clearly seen from the curve for $R = 0.1$. Further, the smaller the Reynolds number, the longer the acceleration remains small, but then the more rapid is the return to g which also occurs nearer to the crisis time of inertia-less theory ($t = 1$ for a rectangular drop in the slender limit).

The above discussion relates strictly only to the acceleration of the particle at the bottom of the drop. It is also of interest to consider other particles. Plotting vertical acceleration versus particle label ξ along the drop centreline ($y = \eta = 0$), as is done for $R = 0.1$ in Figure 2, reveals an interesting characteristic of the flow in the falling drop.

In the initial stages of fall (not shown), the actual acceleration throughout most of the drop is g , but quickly decreases in the viscosity-dominated time range. During this time, the curves at first show an acceleration increasing with ξ , with the maximum acceleration at the bottom $\xi = 1$.

However, this soon changes and the point of maximum acceleration moves progressively up to a position of the order of $\xi = w_0 \ll 1$ distant from the wall. (Note that physically, in terms of x , this is typically quite far from the wall, though in terms of ξ it appears to be very near the wall.) As this occurs and as the acceleration throughout the lower bulk of the drop approaches g , the maximum acceleration may even exceed g for some time. For the $R = 0.1, w_0/L_0 = 0.2$ case illustrated, the acceleration rises to a value of about $1.03g$ around $t \approx 2$ and $\xi \approx 0.16$ ($4.5 < x < 5$); then subsequently, the maximum acceleration decreases to g , until we effectively reach a steady state with the bulk of the drop in free fall. Decreasing the aspect ratio of the initial drop results in an increase in the peak value of acceleration (e.g. for $w_0/L_0 = 0.1$, acceleration reaches about $1.08g$ around $t \approx 1.8$ and $\xi \approx 0.09$ ($2.5 < x < 3$)), but decreasing the Reynolds number R causes a decrease in this peak value, so that for $R = 0.01, w_0/L_0 = 0.1$ the acceleration in the drop nowhere exceeds g .

Finally, the fluid in the region just below the wall boundary of approximate initial length w_0 has an acceleration that reduces from g at $\xi \approx w_0$, to 0 at the wall $\xi = 0$. This region $0 < \xi < O(w_0)$, occupying a smaller and smaller fraction of the length of the drop as the aspect ratio w_0/L_0 decreases, includes but extends beyond the ‘‘wall boundary layer’’ discussed in Stokes et al. (2000).

In Figure 2 the acceleration profile reaches a steady state by $t = 3$. Reducing the Reynolds number reduces the time period over which the acceleration profile evolves, with the time period approaching the crisis time as $R \rightarrow 0$ (c.f. Figure 1).

3.2. Drop shapes

In Figure 3 we plot, for a range of times t and for $R = 0.1$, the scaled drop width $w(\xi, t)/w_0$ versus the particle label ξ . Similarly in Figure 4 we plot w/w_0 versus distance $L(t) - x$ from the bottom of the drop. The latter plot shows just the portion of the drop furthest from the wall containing the bulk of the fluid mass. Both plots show the drop shape to be effectively unchanging at large time, excepting for an ever-thinning filament connecting the main drop to the wall.

At about $t = 2$, as the acceleration in the bulk of the drop nears g , there is a pinching in of the drop near $\xi \approx w_0$, corresponding to a distance $L(t) - x \approx 2$ from the bottom of the drop and from where the filament extends back to the wall. Referring to Figure 2 we

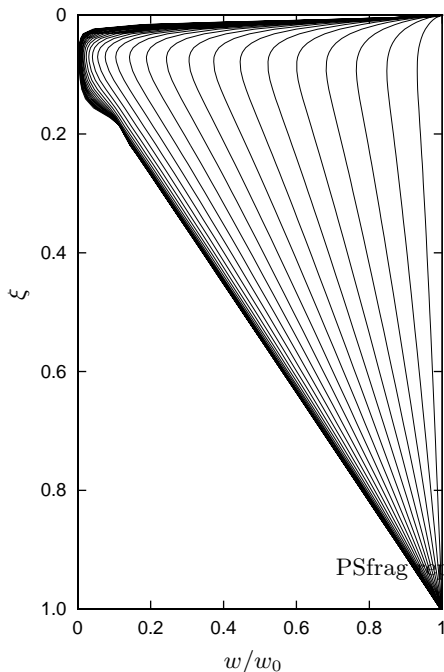


FIGURE 3. Width as a function of ξ , $R = 0.1$, $t = 0, 0.1, 0.2, \dots, 3.0$.

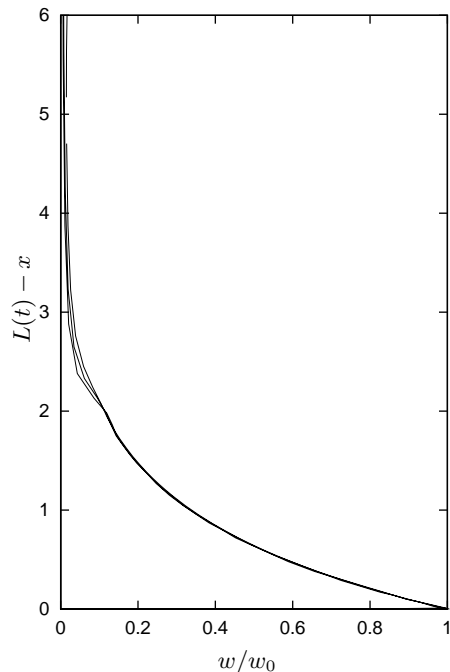


FIGURE 4. Width as a function of $L(t) - x$, $R = 0.1$, $t = 2.0, 2.5, 3.0$, showing that the main drop is effectively a solid body at large time.

see that it is in this filament region that the acceleration decreases from g at the main drop to 0 at the wall, which is to be expected from physical considerations. Because this pinching in occurs once the bulk of the drop has almost reached free fall, it will occur closer and closer to crisis time as $R \rightarrow 0$ and can be associated with the breaking off of the main drop.

This pinching behaviour can be understood with reference to the inertia-less theory (Stokes et al. 2000). In the connecting filament attaching the drop to the wall, viscous forces are still dominant even at large times, so that the acceleration is small and inertia can therefore still be neglected in this region. The main bulk of the drop in virtual free fall below this filament exerts minimal force on the filament, so that we have, effectively, a thin fluid filament extending under the influence of its own mass. Thus, a connecting filament with a free-surface shape similar to those plotted in Stokes et al. (2000) for an initially rectangular drop can be expected. We shall return to this matter later.

4. Slender-drop approximation

Considerable insight into this type of extensional flow can be obtained through an approximate one-dimensional slender-drop analysis. The following development in the main relates to three-dimensional drops where the drop length is much greater than any cross-section width; however, it also applies to two-dimensional drops or sheets where the length is much greater than the sheet thickness.

In a Lagrangian reference frame (Wilson 1988; Stokes et al. 2000) we let $x = X(\xi, t)$, where ξ is a fluid-particle label such that $x = \xi$ at $t = 0$. The initial drop geometry is assumed to have a cross-section area distribution given by some function $A_0(\xi)$. That is,

$A(\xi, 0) = A_0(\xi)$, $0 \leq \xi \leq L_0$, where $A(\xi, t)$ is the cross-sectional area at label ξ and time t , and L_0 is the initial drop length.

Consider a small element of length $dx = X_\xi(\xi_1, t)d\xi_1$ at $\xi = \xi_1$, with volume $dV = A(\xi_1, t)dx$. Conservation of mass demands that dV is time-independent, i.e. $A(\xi_1, t)dx = A_0(\xi_1)d\xi_1$. Since $dx = X_\xi d\xi_1$, we have $AX_\xi = A_0$, which is the differential form of the Lagrangian continuity equation. Integration yields

$$X(\xi, t) = \int_0^\xi \frac{A_0(\xi_1)}{A(\xi_1, t)} d\xi_1 \quad (4.1)$$

as in Stokes et al. (2000).

Newton's second law for this element states that its mass times its downward acceleration is equal to its weight less the net viscous force resisting elongation. The latter viscous force can be written as stress σ times area A on the top side $\xi = \xi_1$ minus that on the bottom side $\xi = \xi_1 + d\xi_1$. Thus if $a = a(\xi_1, t) = X_{tt}(\xi_1, t)$ is the downward acceleration,

$$(\rho dV)a = (\rho dV)g + \left[\sigma A \right]_{\xi=\xi_1}^{\xi=\xi_1+d\xi_1}. \quad (4.2)$$

Using the continuity requirement $dV = Adx = A_0 d\xi_1$ as above, and summing over all elements $\xi = \xi_1$ lying below station ξ , assuming zero stress $\sigma = 0$ at the bottom $\xi = L_0$ of the drop, we have

$$\begin{aligned} \int_\xi^{L_0} \rho [g - a(\xi_1, t)] A_0(\xi_1) d\xi_1 &= \sigma(\xi, t)A(\xi, t) \\ &= -\mu^* \frac{\partial}{\partial t} A(\xi, t). \end{aligned} \quad (4.3)$$

In the above, μ^* is the elongational (Trouton) viscosity (Bird 1977, p. 30), namely $\mu^* = 3\mu$ in three dimensions and $\mu^* = 4\mu$ in two dimensions, which relates stress σ and elongational rate of strain $-A_t/A$. Integrating (4.3) with respect to time t gives

$$A(\xi, t) = A_0(\xi) - \frac{\rho}{\mu^*} \int_\xi^{L_0} A_0(\xi_1) [gt - u(\xi_1, t)] d\xi_1. \quad (4.4)$$

where $u(\xi_1, t) = X_t(\xi_1, t)$ is the downward velocity of the element at $\xi = \xi_1$.

Equation (4.4) is the appropriate generalisation of the corresponding inertia-less equation in Stokes et al. (2000), namely that resulting from dropping the term in u , and is to be solved together with the continuity equation (4.1).

Equivalent Eulerian equations are also not difficult to construct. Defining a small slenderness parameter (in 3D) as the maximum value of $\sqrt{A_0(x)}/L_0$, a formal asymptotic expansion of (2.1) and (2.2) with respect to this parameter yields equations for the velocity $u(x, t)$ and cross-section area $A(x, t)$, namely a ‘‘one-dimensional Navier-Stokes equation’’

$$\frac{\partial u}{\partial t} + u \frac{\partial u}{\partial x} = g + \nu^* \frac{1}{A} \frac{\partial}{\partial x} \left(A \frac{\partial u}{\partial x} \right) \quad (4.5)$$

($\nu^* = \mu^*/\rho$), and a one-dimensional continuity equation

$$\frac{\partial A}{\partial t} + \frac{\partial}{\partial x} (Au) = 0. \quad (4.6)$$

Equations equivalent to (4.5) and (4.6) were given by Kaye (1991). In practice, the Lagrangian system (4.4) and (4.1) is much easier to solve. However, the presence of the term in $u = X_t$ in (4.4) couples the two Lagrangian equations and variables X and A

together, which means that the solution is no longer just a pair of quadratures, as it was in Stokes et al. (2000).

4.1. Nonlinear diffusion equations

We proceed by differentiating (4.4) with respect to ξ , dividing through by $A_0(\xi)$, and then differentiating again with respect to ξ to give

$$\frac{\partial}{\partial \xi} \left[\frac{1}{A_0} \frac{\partial}{\partial \xi} (A - A_0) \right] = -\frac{1}{\nu^*} \frac{\partial u}{\partial \xi}. \quad (4.7)$$

Differentiating (4.1) with respect to t and ξ gives u_ξ in terms of A , and substituting into (4.7) finally yields

$$\frac{\partial A}{\partial t} = \nu^* \frac{A^2}{A_0} \frac{\partial}{\partial \xi} \left[\frac{1}{A_0} \frac{\partial}{\partial \xi} (A - A_0) \right]. \quad (4.8)$$

For any given initial drop shape $A_0(\xi)$, we must solve equation (4.8) for $A(\xi, t)$ subject to the initial condition

$$A(\xi, 0) = A_0(\xi). \quad (4.9)$$

The boundary condition at the bottom (free) end of the drop $\xi = L_0$ is just

$$A(L_0, t) = A_0(L_0), \quad (4.10)$$

obtained by setting $\xi = L_0$ in (4.4) and equivalent to the Eulerian zero-stress condition $u_x = 0$. The zero normal-velocity boundary condition $u = 0$ at the wall end $\xi = 0$ is

$$\frac{\partial A}{\partial \xi}(0, t) = A'_0(0) + \frac{g}{\nu^*} A_0(0)t \quad (4.11)$$

obtained by differentiating (4.4) with respect to ξ and setting $\xi = 0$. The zero tangential-velocity boundary condition $v = 0$ at the wall is by necessity violated in this slender-drop approximation; when included it induces a wall boundary layer, as discussed in Stokes et al. (2000). Once $A(\xi, t)$ is found, we use the continuity equation (4.1) to find $X(\xi, t)$, and hence the drop length $L(t) = X(L_0, t)$.

A suitable non-dimensional form of this problem follows by scaling $A(\xi, t)$ and $A_0(\xi)$ with respect to $A_0(0)$, ξ with respect to L_0 , and t with respect to $\nu^*/(gL_0)$. Then equation (4.8) becomes

$$\frac{A^2}{A_0} \frac{\partial}{\partial \xi} \left[\frac{1}{A_0} \frac{\partial (A - A_0)}{\partial \xi} \right] = R \frac{\partial A}{\partial t}, \quad (4.12)$$

where R is defined by equation (3.5).

The special case of an initially-cylindrical drop with $A_0(\xi) = 1$ simplifies (4.12) to

$$A^2 \frac{\partial^2 A}{\partial \xi^2} = R \frac{\partial A}{\partial t}. \quad (4.13)$$

Equation (4.13) is a nonlinear diffusion equation with a diffusivity proportional to the square of the ‘‘concentration’’ A , and is to be solved in $0 < \xi < 1$ with initial condition $A = 1$ at $t = 0$, and boundary conditions $A = 1$ at $\xi = 1$, and $\partial A / \partial \xi = t$ at $\xi = 0$. This equation was derived by Kaye (1991) (equation (4.3.20), p. 72) from an Eulerian formulation. Although there are methods (see e.g. Ames 1972, p.14) for converting (4.13) to a linear diffusion equation, and hence solving analytically, these solutions are not appropriate for the present boundary conditions, and we shall instead use direct numerical methods.

The inertia-less limit is $R = 0$, and in that limit the solution of (4.13) subject to these

boundary conditions is simply

$$A(\xi, t) = 1 - t + t\xi \quad (4.14)$$

corresponding to a drop length

$$L(t) = -t^{-1} \log(1 - t) \quad (4.15)$$

which becomes infinite at the (scaled) crisis time $t = 1$. However, we expect that for any finite R the drop length remains finite for all finite t , and that for large t the acceleration approaches gravity, which means that $RL''(t) \rightarrow 1$.

4.2. Slender-drop numerical computations

In the general case, it is convenient to define $B(\xi, t) = A(\xi, t) - A_0(\xi)$ as the departure from the initial shape $A_0(\xi)$. Then (4.12) is a nonlinear diffusion equation for B , with diffusivity proportional to $A^2 = (A_0 + B)^2$.

We have for the present purpose solved (4.12) numerically, and indeed have not found it necessary to use anything other than the most direct explicit finite-difference method, i.e. with time step Δt and space step $\Delta \xi$, we approximate (4.12) by

$$B(\xi, t + \Delta t) = B(\xi, t) + C \left[\frac{B(\xi + \Delta \xi, t) - B(\xi, t)}{A_0(\xi + \Delta \xi/2)} - \frac{B(\xi, t) - B(\xi - \Delta \xi, t)}{A_0(\xi - \Delta \xi/2)} \right] \quad (4.16)$$

where

$$C = \frac{\Delta t A(\xi, t)^2}{R \Delta \xi^2 A_0(\xi)}. \quad (4.17)$$

The boundary conditions are $B = 0$ at $t = 0$ and $\xi = 1$, and $\partial B / \partial \xi = t$ at $\xi = 0$; the latter is implemented simply by defining an artificial value $B(-\Delta \xi, t) = B(\Delta \xi, t) - 2t\Delta \xi$ for use in the last term of (4.16) at $\xi = 0$.

The Courant number C must be kept less than 0.5 for stability, which presents no problems with respect to nonlinearity since the cross-section area $A = A_0 + B$ tends to reduce from its initial value, but does present a few problems when R is small, which is of course the most interesting case. In practice however, there appear to be no barriers to use of extremely small time steps Δt when R is small. We have generally found that $\Delta \xi \approx 0.02$ gives adequate spatial accuracy; but then for example with $R = 0.001$ we need $\Delta t \approx 10^{-7}$ for stability.

The actual results for $A(\xi, t)$ are simple and well behaved. For example, for the initially-rectangular case shown in Figure 5, the cross-section area at first reduces steadily and almost linearly with respect to both time t and spatial label ξ , as in the inertial-less limit (4.14). Near $t = 1$ and $\xi = 0$ (i.e. at the wall) the rate of this reduction slows down and then A slowly approaches zero at $\xi = 0$ as time further increases.

It appears from our computations for this case that $A(\xi, t) \rightarrow \xi$ as $t \rightarrow \infty$, as indicated in Figure 5, in agreement with a large-time asymptotic theory to be discussed below. Kaye (1991) conjectured (based on a relatively-coarse discretisation) that the wall value of A would go negative at a finite time t identifiable as that for breaking, but we have found no such event, and believe that breaking cannot occur in the present model for any $R > 0$, and that A must remain positive.

Equating A with drop width w in two-dimensions, we see that there is good comparison between the slender-drop results shown in Figure 5 and our earlier finite element results shown in Figure 3. Noting that the main drop shape below the filament given by our finite element computations appears to approach

$$w/w_0 = (\xi - w_0/2)/(1 - w_0/2) \quad (4.18)$$

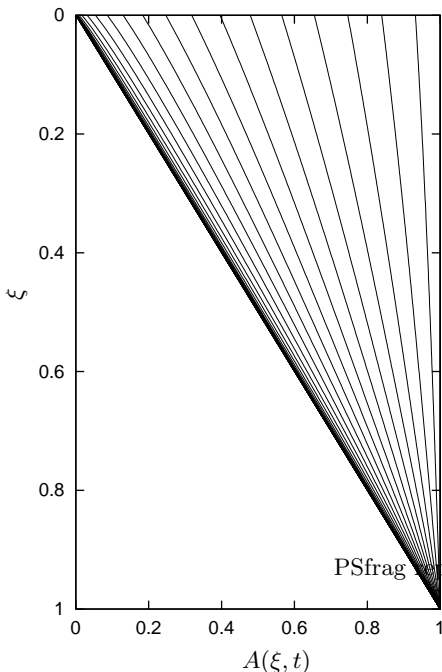


FIGURE 5. Slender drop cross-section area A as a function of ξ , $R = 0.1$, $t = 0, 0.1, 0.2, \dots, 3.0$.

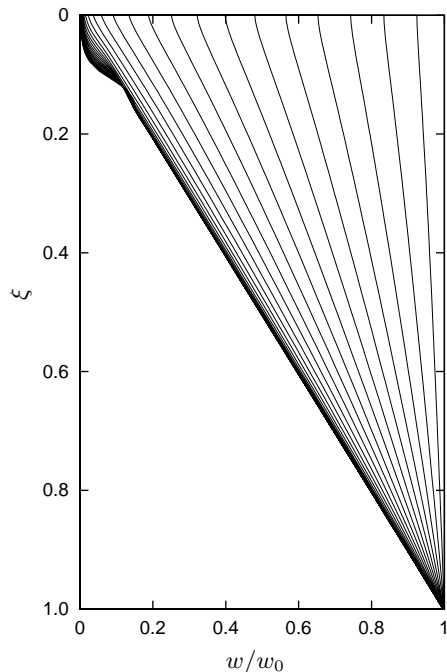


FIGURE 6. Width as a function of ξ , $R = 0.1$, $t = 0, 0.1, 0.2, \dots, 3.0$. Finite element computation, $w/w_0 = 0.2$, slip wall boundary.

as $t \rightarrow \infty$, we retrieve the slender drop result $w/w_0 \rightarrow \xi$ as $w_0 \rightarrow 0$. The pinching in of the filament seen in finite-element simulations at $\xi \approx w_0$ will not be observable in the slender-drop limit but can be associated with the large slope $\partial A/\partial \xi$ that develops at large time at $\xi = 0$ as indicated by (4.11). It is tempting to attribute the differences seen between Figures 3 and 5 to the fact that slip is necessarily permitted along the wall in the slender-drop theory which is not permitted in finite-element simulations. Certainly this results in a wall boundary layer in Figure 3 which is absent in Figure 5. However, this cannot extend the length of the filament and explain the pinching in of the filament just above the main drop.

This is emphasised by running a finite-element simulation with wall boundary conditions of no normal velocity and no tangential stress, thus allowing slip along the wall similar to the slender-drop theory, Figure 6. Again we have a pinching in of the filament, but near $\xi = w_0/2$ not $\xi = w_0$, which clearly demonstrates that this is a finite-width effect rather than a consequence of a no-slip wall boundary, though the no-slip boundary does increase the distance of the pinching position from the wall by the thickness of the boundary layer $O(w_0/2)$. It is very interesting to note that the large-time shape of the drop below the filament (see Figure 6) appears to be $w/w_0 \rightarrow \xi$ just as for the slender-drop theory. Thus, with a no-slip wall boundary, the deviation of the main drop shape from $w/w_0 \rightarrow \xi$ to (4.18), is attributable to the wall effect, as it was in the inertia-less case (Stokes et al. 2000).

Returning to our slender-drop theory, once we have solved for $A(\xi, t)$, other flow variables follow, in particular the acceleration as measured by the second derivative of the drop length. This is computed from $A(\xi, t)$ by evaluating the velocity $u(\xi, t)$ by numerical ξ -differentiation of (4.4), followed by numerical t -differentiation of the bottom velocity

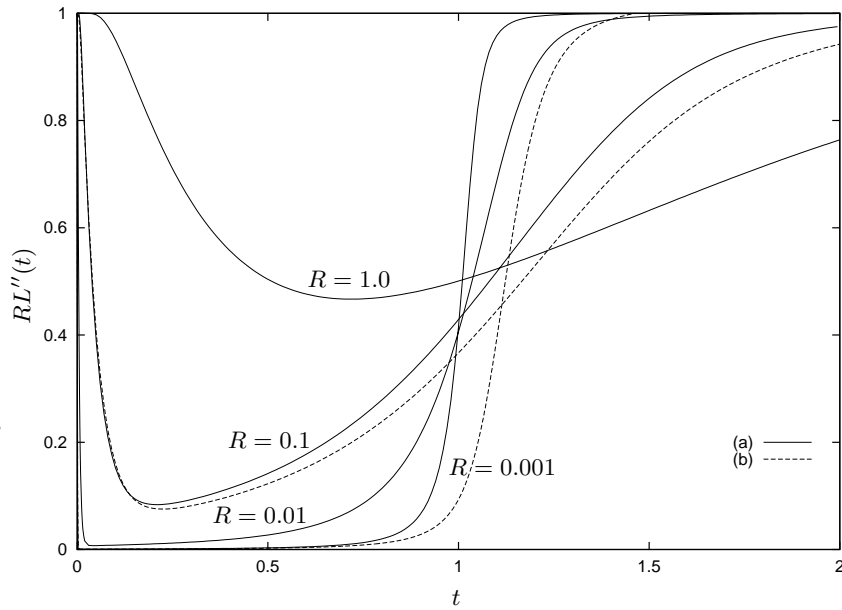


FIGURE 7. Acceleration $RL''(t)$ versus time t for an initially cylindrical slender drop. (a) Slender drop theory and (b) finite-element curves from Figure 1.

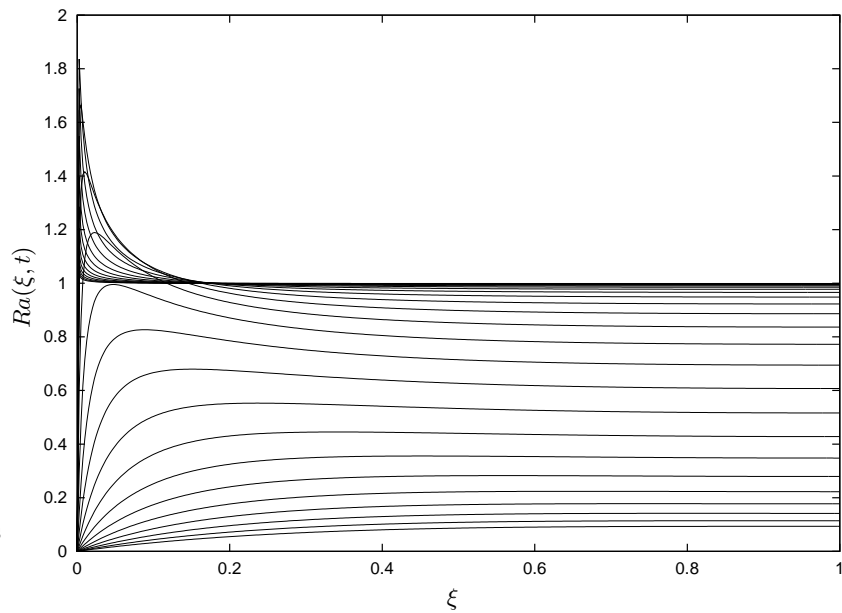


FIGURE 8. Acceleration as a function of initial position ξ in the slender drop limit, $R = 0.1$, $t = 0.2, 0.3, \dots, 3.0$.

$u(1, t) = L'(t)$. In Figure 7 we plot $RL''(t)$ versus time for various values of R , for an initially rectangular slender drop. As with the finite-element results, this quantity starts and ends at 1 with a viscosity-dominated time period in between. As before, reducing R causes the rise in acceleration near $t = 1$ to become steeper and steeper and to approach closer and closer to the inertia-less crisis at $t = 1$. The curves from the finite-element

computations for an initially rectangular drop of aspect ratio $w_0/L_0 = 0.2$, also shown (dashed) on Figure 7, compare well with their slender-drop theory counterparts and show a delay in the return to $RL''(t) = 1$ as the effect of the no-slip wall boundary.

Of even more interest is the acceleration profile in the drop, as a function of ξ , in the slender drop limit. This is shown over a range of times in Figure 8. As in the finite-element calculations we find that, after a relatively short time, the acceleration takes its maximum value at a position in the interior of the drop for a considerable time, with this position moving towards the wall as time progresses. However, the maximum acceleration is very much larger than in the finite-element computations and, in fact, due to limitations on the spatial grid near $\xi = 0$, we have not been able to determine just how large it becomes, but only that it increases as our grid resolution at the wall decreases. Further, the position of maximum acceleration appears to approach the wall, whereas in our finite-element computations it only came as close as the transition region between the main drop and the filament.

Finally, in the slender-drop limit, the acceleration versus ξ curve appears to approach the step function $Ra(\xi, t) = 1$, $1 \leq \xi < 0$, $Ra(0, t) = 0$ as $t \rightarrow \infty$, as seen in Figure 8, with no progressive decrease in acceleration from g at $\xi = w_0$ to 0 at $\xi = 0$, as occurred in the finite-element computations. This seems to be associated with the fact that pinching in of the connecting filament occurs at $\xi = 0$ in the slender limit with the whole of the drop effectively going into free fall, and implies that the drop then breaks at the wall.

4.3. Initially paraboloidal drops

Although the example of an initially-rectangular 2D drop is used for simplicity in the above, it is not particularly realistic as a model of real drops. An example of an initial drop shape which is reasonably realistic is that for which $A_0(\xi) = 1 - \xi$. In the 3D axisymmetric case, this drop has an initially paraboloidal shape, with radius proportional to $\sqrt{1 - \xi}$. Figure 9 shows the computed $A(\xi, t)$ for this case at $R = 0.1$, plotted at time intervals of 0.2 up to $t = 3.6$. Note that the inertia-less theory ($R = 0$) predicts a scaled crisis time of $t = 2$ for this case. As with the initially-rectangular drop, at first the output $A(\xi, t)$ decreases essentially linearly with t , but this decrease slows near to the crisis time, and then it appears that $A(\xi, t) \rightarrow \xi(1 - \xi)$ as $t \rightarrow \infty$.

The actual axisymmetric drop shapes in the physical plane are shown in Figure 10 by plotting $x = X(\xi, t)$ versus $r = \sqrt{A(\xi, t)}$. This time history seems quite sensible, and in particular demonstrates for large time an approach to a freely falling state which we now discuss.

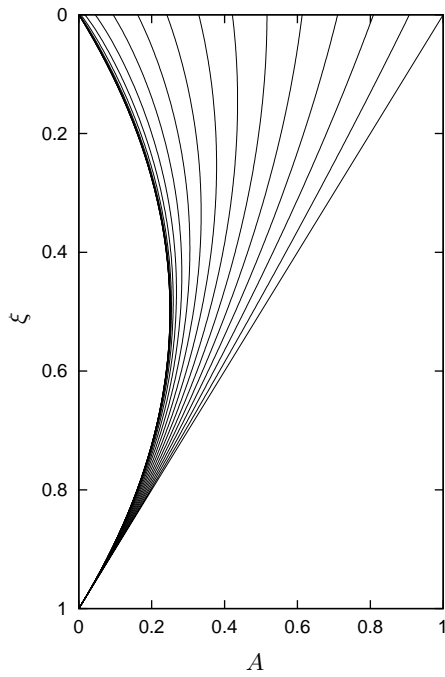


FIGURE 9. Drop cross-section area A as a function of particle label ξ , for initially paraboloidal drop $A_0(\xi) = 1 - \xi$, at Reynolds number $R = 0.1$, for times $t = 0, 0.2, 0.4, \dots, 3.6$.

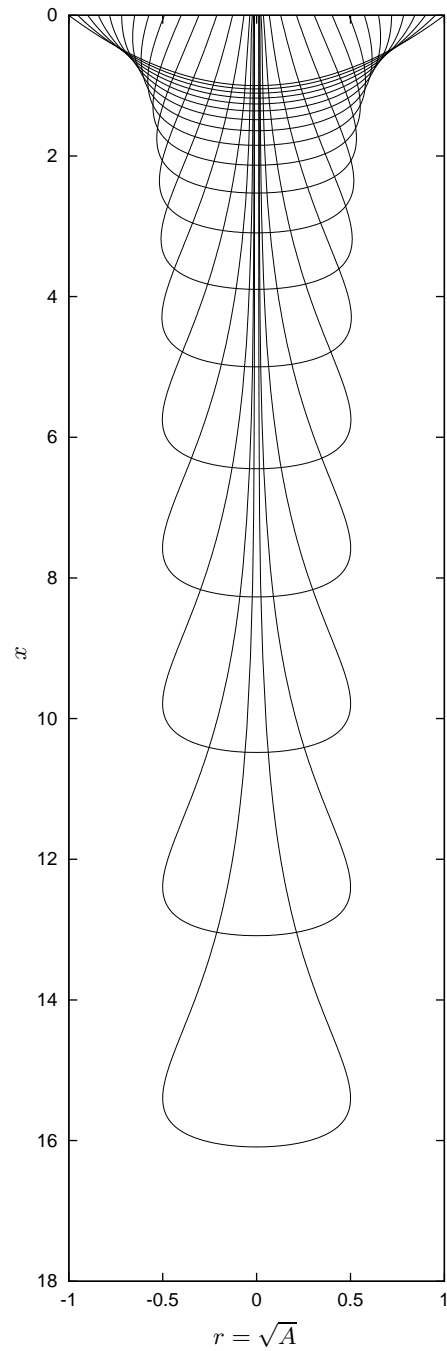


FIGURE 10. Evolution of the initially paraboloidal drop of Figure 9, as seen in physical coordinates x, r .

4.4. Large-time drop shape

An intuitive argument for the large-time behaviour is as follows, reverting temporarily to unscaled variables.

Once the drop is in free fall as if it were a rigid body, its velocity must be of the form

$$u(\xi, t) = g(t - t_0) \quad (4.19)$$

for some constant t_0 , physically interpretable as the apparent time when this free fall begins. Because of the initial slowing down of motion due to viscosity, we expect $t_0 > 0$, but otherwise in principle the quantity t_0 is unknown in advance.

However, when fluid inertia has only a small effect, i.e. for relatively small R , we may expect that $t_0 = t^*$, where t^* is the crisis time (when formally the inertia-less theory (Stokes et al. 2000) predicts breaking), because then close to the crisis time, the acceleration of the drop (excepting a small region near the wall) rapidly approaches g and remains at that value thereafter. Prior to this event, all fluid velocities $u(\xi, t)$ were small, and from a large- t viewpoint we may assume that the drop was then at rest.

If we substitute (4.19) into (4.4), we find

$$A(\xi, t) = A_0(\xi) - \frac{g}{\nu^*} t_0 V(\xi) \quad (4.20)$$

where

$$V(\xi) = \int_{\xi}^{L_0} A_0(\xi_1) d\xi_1 \quad (4.21)$$

is the volume of drop fluid below station ξ .

Now in the present slender-drop theory, there is slip at the wall, and for a large family of initial drop shapes, including those considered above, it appears that the wall thickness tends to zero at large times. If therefore we demand that $A = 0$ at $\xi = 0$ in (4.20), we find

$$t_0 = \frac{\nu^* A_0(0)}{g V(0)} \quad (4.22)$$

so

$$A(\xi, t) = A_0(\xi) - \frac{A_0(0)}{V(0)} V(\xi) . \quad (4.23)$$

It happens that (4.22) is the correct formula for the crisis time t^* in the inertia-less theory of Stokes et al. (2000), for those initial drops that break at the wall according to that theory, confirming that $t_0 = t^*$ when R is small.

Indeed, we expect that $t_0 \approx t^*$ in all cases, whether or not inertia is small, and whether or not the drop breaks at the wall, but this is not yet proved. In any case there appears to be a remarkable relationship between the inertia-less theory and the large-time limit of the flow with inertia. Namely, as $t \rightarrow \infty$ in a computation including inertia, the drop shape approaches that which would have been obtained at the (finite) crisis time $t = t^*$ in a computation neglecting inertia.

For an initially cylindrical drop $A_0 = 1$, with $V(\xi) = 1 - \xi$ (in scaled form), equation (4.23) predicts $A \rightarrow \xi$ as $t \rightarrow \infty$. Similarly, for the initially paraboloidal drop $A_0 = 1 - \xi$, with $V(\xi) = (1 - \xi)^2/2$, we have $A \rightarrow \xi(1 - \xi)$. Both of these limits are confirmed by our computations.

The actual final drop shape as a function of the physical coordinate $x = X(\xi, t)$ is obtained by integrating the continuity equation $X_{\xi} = A_0/A$. However, this integration cannot be (as with (4.1)) from the wall $\xi = 0$, where (4.23) has $A = 0$, because this integral diverges. Of course it must so diverge, since at infinite times the drop is an

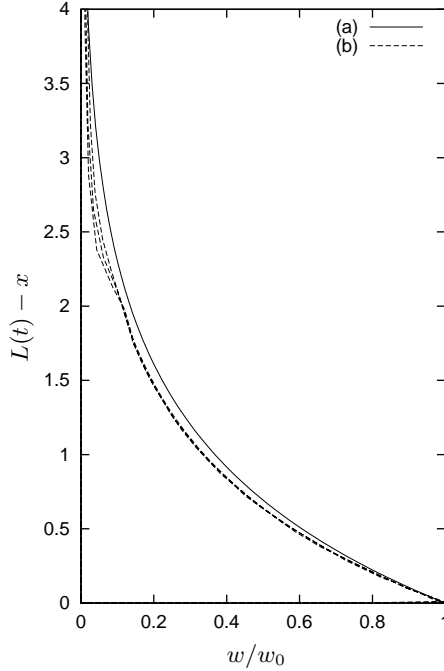


FIGURE 11. Drop width as a function of $L(t) - x$ at large time t for an initially rectangular drop, $R = 0.1$. Comparison of (a) slender-drop theory and (b) finite-element computation, $w_0/L_0 = 0.2$.

infinite distance from the wall! If instead we integrate from the bottom $\xi = L_0$, using the asymptotic estimate (4.23) for $A(\xi, t)$, we find

$$X(\xi, t) = L(t) - \int_{\xi}^{L_0} \frac{A_0(\xi_1) d\xi_1}{A_0(\xi_1) - [A_0(0)/V(0)]V(\xi_1)}. \quad (4.24)$$

Equations (4.23) and (4.24) provide the formal connection between initial and final drop shapes.

For example, a drop with $A_0 = (1 - \xi)^n$ for any n (including both the initially rectangular and paraboloidal cases) gives $X = L(t) + \log \xi$, or $\xi = e^{-(L-x)}$. Thus the asymptotic radius of this family of drops is \sqrt{A} where

$$A = e^{-(L-x)} [1 - e^{-(L-x)}]^n, \quad (4.25)$$

an explicit function of distance $L(t) - x$ measured upward from the bottom of the drop. Then, in two dimensions where $w \equiv A$, setting $n = 0$ for the initially rectangular drop, we have $w/w_0 = e^{-(L-x)}$ in close agreement with the shapes shown in Figure 4. Figure 11 shows just how good this agreement is for an initial aspect ratio of $w_0/L_0 = 0.2$, and the comparison is almost identical for $w_0/L_0 = 0.1$. For the initially paraboloidal drop ($n = 1$) we have $r = \sqrt{A} = \sqrt{e^{-(L-x)} [1 - e^{-(L-x)}]}$, which corresponds closely to the large-time drop shape seen in Figure 10. This final drop takes a maximum width 0.5 (times the original maximum width) at a distance $\log 2 = 0.693$ (times the original length) above the bottom, and its thickness then decays exponentially at greater distances above the bottom.

The present asymptotic theory does not quite provide an estimate of the actual bottom position $x = L(t)$, although equation (4.19) gives an estimate of its time derivative

$L'(t) = u(L_0, t)$. Further work would be needed to estimate the constant of integration, i.e the apparent initial length $L(t) - g(t - t_0)^2/2$.

In summary, the asymptotic theory of the present section enables estimates of the shape of the drop in its “final” freely-falling rigid-body-like state, given any initial shape. There must also be a fine filament connecting this drop to the wall, whose thickness reduces with time. The above description applies until surface tension breaks the filament, and eventually (after a sufficient time in free fall) converts any 3D drop into a sphere.

5. The filament

Comparisons of finite-element computations for drops of finite width with results from the slender-drop theory do show a difference in the filament behaviour and further work is required to determine exactly what is happening for small ξ . Nevertheless, for drops of finite width the computations show the main drop beginning to pinch off from the thin filament, even in the absence of surface tension in the problem formulation. In the slender-drop limit we infer that this happens at the wall itself, but in practice it happens beyond a thin wall boundary layer. We can expect that surface tension will play a significant role in the vicinity of this pinching zone, and will finally determine the exact breaking position, but we suggest that the present theory neglecting surface tension yields a good indication of this position. In the inertia-less limit, pinching of the filament is not seen, due to the fact that we cannot compute beyond the crisis time, and the approximate position of drop break-off is determined as in Stokes et al. (2000), being at the wall itself for the drops considered above. Thus, in the slender-drop limit, inclusion of inertia makes no difference to the predicted position of break-off, but for drops of finite width this matter needs further investigation.

We might argue that for $t \geq t_0$, the acceleration is just g throughout the main freely falling drop below $\xi = L_f$, for some L_f marking the boundary between filament and main drop. Then (4.3) becomes

$$-\mu^* \frac{\partial}{\partial t} A(\xi, t) = \int_{\xi}^{L_f} \rho [g - a(\xi_1, t)] A_0(\xi_1) d\xi_1 \quad (5.1)$$

and, hence,

$$A(\xi, t) = A(\xi, t_0) - \frac{1}{\nu^*} \int_{\xi}^{L_f} [g(t - t_0) - (u(\xi_1, t) - u(\xi_1, t_0))] A_0(\xi_1) d\xi_1. \quad (5.2)$$

But, in the filament $0 \leq \xi \leq L_f$ it seems reasonable to neglect inertia, drop the terms in $u(\xi, t)$ and use the inertia-less theory and results given in Stokes et al. (2000). In particular, the time and location of filament breaking are determined by the filament shape at $t = t_0$, as is its subsequent shape. However, while we may thus explain the filament behaviour as seen in our finite-element computations above, any meaningful analysis of the ultimate behaviour of these very thin filaments must include surface tension.

6. Conclusion

By including inertia terms in the flow model, both in a slender-drop approximation and in an exact computation, we have demonstrated how, in both the very early and very late stages of the fall of a drop of viscous fluid, the drop’s acceleration becomes equal to the gravitational acceleration g . In the intervening period, from soon after it

begins its descent until a “crisis” time when a rapid increase occurs, accelerations are small compared to gravity, and neglect of inertia is valid for small values of the parameter $R = gL_0^3/\nu^{*2}$. The crisis time $t^* = O(\nu^*/(gL_0))$ computed from the inertia-less theory is then a good estimate of the time at which the drop acceleration increases rapidly toward g , when we can expect the drop to break and go into free fall.

Drop shapes are available from the exact or slender-drop computations at all times and for all Reynolds numbers. However, the slender-drop theory also provides explicit formulae via simple quadratures for the final quasi-rigid-body shape of the drop when it is in free fall prior to smoothing by surface tension, this shape being the same as the inertia-less theory predicts at the finite crisis time.

Including inertia also provides insight into the behaviour of the ever-thinning filament which connects this ultimate drop to the wall, prior to breaking events controlled by surface tension.

This work was supported by the Australian Research Council through a Postdoctoral Fellowship to YMS and a grant to EOT. The authors acknowledge valuable discussions with Prof. P. Broadbridge.

REFERENCES

- AMES, W.F. 1972 *Nonlinear Partial Differential Equations in Engineering*. Interscience, New York.
- BIRD, R.B., CURTISS, C.F., ARMSTRONG, R.C. & HASSAGER, O. 1977 *Dynamics of Polymeric Liquids, v.1 Fluid Mechanics*. Wiley, New York.
- CRAM, L.E. 1984 A numerical model of droplet formation. In *Computational Techniques and Applications: CTAC-83* (ed. J. Noye & C. Fletcher), pp. 182–188. Elsevier, North-Holland.
- CSIRO 1999 *Fastflo version 3, Tutorial Guide*. Commonwealth Scientific and Industrial Research Organisation (CSIRO), Australia.
- EGGERS, J. 1993 Universal pinching of 3D axisymmetric free surface flow. *Phys. Rev. Lett.* **71**, 3458–3460.
- HENDERSON, D., SEGUR, H., SMOLKA, L.B. & WADATI, M. 2000 The motion of a falling liquid filament. *Phys. Fluids* **12**, 550–565.
- KAYE, A. 1991 Convected coordinates and elongational flow. *J. Non-Newtonian Fluid Mech.* **40**, 55–77.
- PAPAGEORGIOU, D.T. 1995 On the breakup of viscous liquid threads. *Phys. Fluids* **7**, 1529–1544.
- SARKAR, K. & SCHOWALTER, W.R. 2001 Deformation of a two-dimensional drop at non-zero Reynolds number in time-periodic extensional flows: numerical simulation. *J. Fluid Mech.* **436**, 177–206.
- STOKES, Y.M., TUCK, E.O. & SCHWARTZ, L.W. 2000 Extensional fall of a very viscous fluid drop. *Quart. J. Mech. Appl. Math.* **53**, 565–582.
- WILKES, E.D., PHILLIPS, S.D. & BASARAN, O.A. 1999 Computational and experimental analysis of dynamics of drop formation. *Phys. Fluids* **11**, 3577–3598.
- WILSON, S.D.R. 1988 The slow dripping of a viscous fluid. *J. Fluid Mech.* **190**, 561–570.